Application of NDT active thermography for the characterization of the cold spray process of high entropy alloys

Nondestructive Testing and Evaluation

ISSN: (Print) (Online) Journal homepage: www.tandfonline.com/journals/gnte20

Application of NDT active thermography for the characterisation of the cold spray process of high-entropy alloys

Raffaella Sesana, Luca Corsaro, Nazanin Sheibanian & Sedat Özbilen

To cite this article: Raffaella Sesana, Luca Corsaro, Nazanin Sheibanian & Sedat Özbilen (19 Nov 2024): Application of NDT active thermography for the characterisation of the cold spray process of high-entropy alloys, Nondestructive Testing and Evaluation, DOI: 10.1080/10589759.2024.2430378

To link to this article: https://doi.org/10.1080/10589759.2024.2430378

Published online: 19 Nov 2024.

NONDESTRUCTIVE TESTING AND EVALUATION
https://doi.org/10.1080/10589759.2024.2430378

Taylor & Francis
Taylor & Francis Group

Application of NDT active thermography for the characterisation of the cold spray process of high-entropy alloys

Raffaella Sesana[a], Luca Corsaro[a], Nazanin Sheibanian[a,b] and Sedat Özbilen[c]

[a]Department of Mechanical and Aerospace Engineering, Politecnico di Torino, Torino, Italy; [b]TSUBAKI NAKASHIMA Central Laboratory (TN ITALY), Pinerolo, Torino, Italy; [c]Department of Mechanical, Manufacturing & Biomedical Engineering, Trinity College Dublin, the University of Dublin, Dublin, Ireland

ABSTRACT

A Non-Destructive technique (NDT) based on Active Thermography (AT) is proposed to correlate mechanical properties, process parameters and thermal response for High-Entropy Alloys (HEA) coatings. More in detail, the Pulsed technique is utilised to investigate thermal responses generated by different High-Entropy Alloys (HEA) coatings. In particular, specimens tested in this work are made of several chemical compositions ($Al_xCoCrCuFeNi$ and MnCoCrCuFeNi) and are realised by using different Cold Spray temperatures (650°C, 750°C and 850°C), generating coatings with various mechanical properties. This way, results in terms of thermal responses obtained with a Non-Destructive technique are correlated, by means of ANOVA, with the corresponding chemical compositions and process parameters of each specimen. The impact of both roughness and emissivity on the process characterisation was also investigated.

ARTICLE HISTORY
Received 28 February 2024
Accepted 12 November 2024

KEYWORDS
High entropy alloy; cold spray; NDT; active thermography; process characterisation

1. Introduction

To protect a part or structure exposed to mechanical or chemical damage, a variety of coating methods and materials are available. As a result of this protective function, manufacturing costs are reduced. Various coating materials are available, including metallic alloys, ceramics, bio-glasses, polymers, and engineered plastics, which provide designers with a wide selection of options for durable protection [1]. They can provide effective protection to the underlying materials against aggressive environments such as wear, corrosion, and high temperature. It is considered that HEAs (High-Entropy Alloys) are candidates for coating materials due to their versatile and superior properties over conventional metals and alloys [2].

HEAs are composed of multiple and equiatomic metal elements, such as Fe, Co, Ni, Cr, Mn, Mo, Al, Ti [3,4]. In general, HEAs can present excellent properties, in many cases better than conventional alloys: high strength and hardness, considerable resistance to wear, exceptional resistance in conditions of high temperature, good structural stability and excellent resistance to corrosion and oxidation [4]. They are of great interest for

CONTACT Luca Corsaro luca.corsaro@polito.it

applications in many industrial fields, particularly in areas where the material is subjected to harsh conditions. Among the numerous HEAs, FeCoNiCrMn with FCC structure exhibits great potential in cryogenic and high-temperature applications, as well as corrosion-/wear-resistance fields [5–9]. A variety of thermal spraying techniques have recently been applied to fabricate HEA coatings for substrate protection, such as laser cladding [10], high-velocity air/oxygen fuel sprays [11,12], magnetron sputtering [13], plasma spraying [14], and plasma cladding [15]. A study by Xiao et al. [14] investigated the tribological properties of plasma sprayed FeCoNiCrMn coatings before and after annealing and concluded that the coatings exhibited rather high wear-resistance performance, which could be further enhanced by annealing.

As a result of the differences between the coatings generated by Cold Spray (CS) technique and those generated by other methods, CS may be considered a viable technology for the repair and even the manufacture of self-standing components. CS refers to a method of the thermal spraying for the production of coatings with similar properties and behaviours to bulk materials. The cold spray technique uses high-temperature compressed gases to accelerate microparticles to 300–1200 m/s, which are deposited on substrates at a temperature below the melting point of the particles [16,17]. As a result of the low deposition temperature, defects are not formed that are associated with high temperatures. The use of low temperatures in CS results in unique characteristics [18]. It is possible to maintain the microstructure and properties of the feedstock powders, as well as to prevent oxide formation and any other unfavourable structural changes, thus enhancing the durability of the coatings. During impact, particles deform plastically, resulting in substrate – coating bonding and coating integrity. In case of temperature-sensitive materials, adhesion of coatings can occur in the solid state without causing significant damage to the substrate. Nowadays, in addition to metals, CS is also used to deposit polymers or ceramics, including traditional and advanced materials.

Coating quality is well known to play an important role in determining the mechanical properties and wear resistance of coated contacts [19]. Various methodologies can be employed to investigate the characterisation of coatings depending on the type, composition, and thickness of the coating and its substrate. Hardnesses and roughnesses measurements are widely utilised to estimate mechanical properties and superficial qualities. During the years, a number of research activities were carried out with the objective of investigating the influence of surface roughness on the quality of coatings. As detailed in [20], the roughness, or the topography of the coating, directly influences the functionality of the coating. In the context of icephobic coatings, the utilised processing methods, such as sandblasting or etching, significantly influence the adhesion of ice, affecting the performance of the coating. It is important to note that, with regards to the coatings, the aspect of roughness also plays a significant role for the substrate. These aspects were well-discussed in [21]. In fact, authors focused the attention on the performance of coatings on the basis of the debonding driving force. In particular, the obtained results shown that the debonding driving force decreases with an increase in interface roughness, and three conditions of performance as safe, critical and fail, respectively, were defined on the basis of the debonding driving force. With respect to the characterisation of coating quality, destructive techniques are directly utilised for this purpose. A less-invasive approach for the evaluation of mechanical properties is given by nanoindentation technique and both advantages and potentialities for brittle material are illustrated in

[22]. In particular, a study on deformation transition in materials such as Al_2O_3 and SiC is proposed. For the purpose of measuring some parameters as, for example, coating thickness, indirect non-destructive techniques are considered [23,24].

Among NDT techniques, Active Thermography (AT) techniques became attractive during the last decades due to the advantage of a non-contact and full field technique. A source of external energy is required in order to induce a temperature difference between the specimen and the environment. The energy sources can also be categorised into optical, mechanical, electromagnetic, or other types of excitations. Optical excitation involves delivering energy to the surface through optical devices such as photographic flashes, halogen lamps or laser. In the field of AT, three classical techniques are based on these two excitation modes: lock-in (LT) thermography (for periodic heating) and pulsed (PT) thermography (pulsed or modulated amplitude). In the specific case of defect identification, the scientific literature is full of papers describing methods and algorithms to improve defects [25–28]. Moreover, the potentiality of Pulsed technique to investigate the heat conduction in case of sub-superficial defects is illustrated in [29]. Generally speaking, it is an on-line method of monitoring, large fields with real-time results (empowered by the use of advanced image processing techniques) [25,26,30]. There is no harmful radiation associated with IRT compared to other technologies, such as X-ray imaging. This makes it suitable for repeated and long-term use. Condition monitoring techniques based on IRT require minimal and relatively inexpensive instrumentation.

During the years, Thermography in both Passive and Active configurations was utilised in many research fields related to coatings with the aim to investigate mechanical properties or coating quality. As an example, the quality and the surface performance of several plasma sprayed coatings on the contact fatigue life were investigated by means of the classical Passive Thermography (PT) approach [31]. In this case, the temperature of the contact point was chosen as the optimal infrared signal since the pre-heating is strictly related to the coating failure. For what concerns Active Thermography (AT), interesting topics, such as microscopic cracks or coating adhesions, are discussed in [32] and [33]. In particular, [32] pointed out how thermal maps generated with vibrothermography stimulated by ultrasound allow to detect micro cracks. As a matter of fact, the heat conduction is altered for hidden cracks and, as a consequence, a localised thermal gradient is emphasised. At the same way, an ultrasound excitation with eddy current pulsed thermography is utilised in [33]. In this work, the coating adhesion was deeply investigated since represents a crucial parameter for the quality of coatings. Artificial defects were generated and the so-called Phase Array method was applied. A similar excitation source was adopted in [34]. More in detail, the potentialities of AT using an electromagnetic induction pulsed-phase thermography were adopted for the detection of early marine corrosion. A dedicated Through Coating Imaging was proposed as an alternative approach with respect to laser profilometry for the in-service corrosion detection, sizing and monitoring. Also, in this case, the roughness of the coating became an important indicator for its analysis during the corrosion process. In fact, the corrosion roughness can be estimated by using the proposed approach, since phase profile and standard deviation of phase as a monotonic relation with the exposure time. On the other hand, thickness measurements were also investigated [35] since is an important quality indicator in case of multilayer coatings such as Thermal Barrier Coatings (TBCs). The eddy current thermography was applied and a dedicated algorithm for the thickness evaluation was developed. The analysis of coating quality is also

investigated by means of classical thermal parameters such as thermal diffusivity and conductivity. As an example, in [36] the AT technique is applied to Plasma Sprayed thermal barrier coatings for turbine blades and both thermal diffusivities and thermal conductivities are estimated according to ISO Standards.

Aim of this paper is to investigate the feasibility of Active Thermography technique for the process characterisation of innovative coatings such as High-Entropy Alloy (HEA) coatings. For this study, HEA coatings made of several chemical composition and deposited by using different Cold Spray temperatures were analysed. The process characterisation is performed by using the Pulsed technique with a laser excitation source. Particular attention to the impact of process parameters on both roughness and emissivity, and then on the process characterisation, was dedicated. As a matter of fact, the impact of the process on thermal and roughness data was investigated with literature review documents along with the relation between coating roughness and related thermal emissivity. Moreover, a statistical analysis was also performed to validate experimental results.

2. Materials and methods

Samples adopted in this study were made with a substrate and a HEA coating deposited with CS technique. More in detail, the substrate utilised for each sample was Magnesium, while the HEA coating was generated by varying both HEA chemical composition and CS deposition temperature. Detailed description of deposition techniques and results are reported in [37].

In Figure 1 the tested samples (superficial coating, left side, sample shape, right side) are shown, while in Table 1 the deposition process parameters (HEA chemical compositions and Cold Spray deposition temperatures) are reported for each sample. As a matter of fact, each HEA coating deposited over the magnesium substrate was generated by combining deposition temperatures and chemical compositions (both illustrated in Table 1). In particular, the HEA chemical composition was mainly of $Al_xCoCrCuFeNi$ and MnCoCrCuFeNi, while the deposition temperatures were 650°C, 750°C and 850°C, respectively. More in detail, the aluminium compositions (Alx) utilised were 0.1, 0.2 and 0.5. The defined process parameters were chosen with the aim of exploring a reasonable Cold Spray temperature range, according to literature [16,18], with an appreciable temperature variation, and to investigate the impact of different chemical compositions.

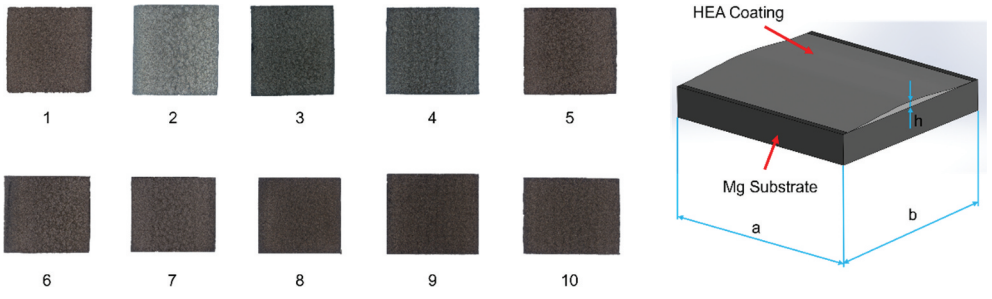

Figure 1. Tested samples (left side) and geometrical shape (right side).

Table 1. Process parameters and geometrical dimensions.

Sample	Chemical composition	Nominal chemical composition in atomic percentage (at%)						Cold Spray Temp. [°C]	Geometrical dimensions [mm]		
		Al	Co	Cr	Cu	Fe	Ni		a	b	h
1	$Al_{0.1}CoCrCuFeNi$	1.96	19.6	19.6	19.6	19.6	19.6	650	10.09	9.39	0.313
2		1.96	19.6	19.6	19.6	19.6	19.6	750	10.01	9.43	0.776
3	$Al_{0.2}CoCrCuFeNi$	3.85	19.2	19.2	19.2	19.2	19.2	650	10.11	9.42	0.507
4		3.85	19.2	19.2	19.2	19.2	19.2	750	10.73	10.01	0.613
5		3.85	19.2	19.2	19.2	19.2	19.2	850	10.72	10.01	0.627
6	$Al_{0.5}CoCrCuFeNi$	9.10	18.2	18.2	18.2	18.2	18.2	650	11.27	10.01	0.497
7		9.10	18.2	18.2	18.2	18.2	18.2	750	11.19	9.97	0.553
8	MnCoCrCuFeNi	16.7	16.7	16.7	16.7	16.7	16.7	650	10.09	9.17	0.386
9		16.7	16.7	16.7	16.7	16.7	16.7	750	10.59	9.21	0.604
10		16.7	16.7	16.7	16.7	16.7	16.7	850	11.73	9.23	0.632

This way, a total number of 10 specimens were generated. Geometrical dimensions of each specimen were measured with an optical microscope ZEISS AXIO Vert.A1 and results are shown in Table 1. More in detail, *a* and *b* dimensions correspond to the superficial substrate dimension, while *h* is the maximum coating thickness measured over the cross section (see Figure 1).

In thermographic measurements, specimen emissivity is affected by many parameters [38] and among them roughness pays a relevant role [39–42]. In [43] the emissivity of two different metals, a Q235 steel and a T2 copper, at different temperatures and roughness was experimentally measured. In particular, for the steel the roughness range is 0.3–6.7 μm while for copper it ranges 0.2–1.1 μm. It resulted that the emissivity of the metals increases with increasing temperature and roughness. Furthermore, the effect of roughness on the emissivity is significant in low temperature, and it is opposite for high temperature. A similar result is obtained for tungsten and rhenium samples in [44] where the relation between roughness and emissivity is negative and the same occurs with temperature. Furthermore, a relation with wavelength and emissivity is confirmed: it is suggested that increasing the roughness, progressively gives more weight to the long-wavelength emissivity in comparison to the short-wavelength ones. In [45] the positive relation between emissivity and surface roughness is demonstrated for cast iron samples, for roughness values between 0.2 and 100 mm and emissivity varying between 0.1 and 0.2 in the 8–14 mm band and a sinusoidal function. The model was implemented by means of AI learning routines.

To take into account of this influence a correlation between thermal response and surface roughness was investigated. Specimen roughness and microstructural characterisation are reported in [4]. More in detail, the roughness measurement results obtained in [4] are reported in Table 2, and measurements were performed by using RPT80 roughness tester (see Figure 2).

The experimental equipment for the specimens is shown in Figure 3. It is composed of an IR thermal camera, a laser excitation source and a PC control unit. The IR thermo camera is a FLIR A6751sc with sensitivity lower than 20 mK and 3–5 μm spectral range, while the laser source can generate a maximum power of 50 W concentrated in a small surface. The reflection mode configuration was adopted (Figure 3(b)), and samples were located 440 mm distance from the thermal camera defining a spatial resolution equal to 0.131 mm/pixel. The maximum frame rate

Table 2. Roughness measurements.

	Ra		*Rq*		*Rt*	
Sample	Average [μm]	Std dev. [μm]	Average [μm]	Std dev. [μm]	Average [μm]	Std dev. [μm]
1	5.912	0.461	7.217	0.560	42.757	2.318
2	4.847	0.432	5.868	0.475	31.201	3.296
3	5.006	0.850	6.083	0.875	31.669	3.826
4	5.860	0.852	7.133	1.064	38.346	9.246
5	5.001	0.410	6.248	0.434	37.219	6.565
6	6.493	0.578	7.675	0.739	39.350	6.196
7	5.732	0.818	6.981	0.927	38.299	8.922
8	5.402	0.592	6.566	0.741	34.733	2.571
9	5.528	0.336	6.681	0.337	33.543	2.123
10	5.698	0.304	6.780	0.392	36.392	6.736

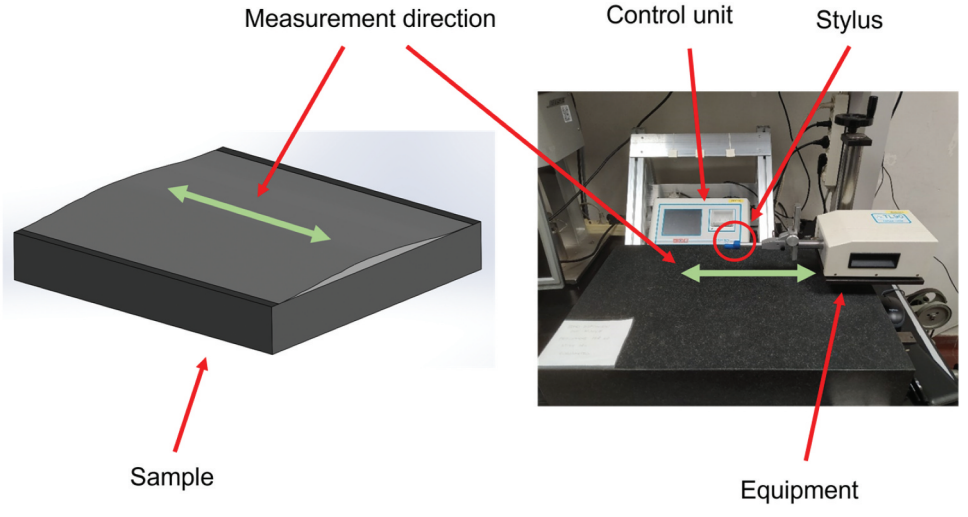

Figure 2. Roughness measurements and equipment.

acquisition was selected, corresponding to 785.67 hz. Environmental conditions (room temperature and humidity) were monitored during each test, while the corresponding reflected temperature was estimated in according to ISO 18,434 Standard [46].

The proposed process characterisation was performed by using the Laser Pulsed technique. More in detail, each sample was thermally excited over the coating zone with a pulse period of 250 ms and with a laser power of 30 W. The diameter of the laser spot is 6 mm and the laser power distribution over the spot has a gaussian distribution. The thermal response was extracted from the thermogram by using an area with 4288 pixel (Region Of Interest, ROI) located over the surface of the tested samples (see Figure 4(a)).

Room radiance was measured on the sample before laser excitation and results in absolute radiance values were processed by using FLIR Research IR software, and a mean value of four replications was considered for each sample.

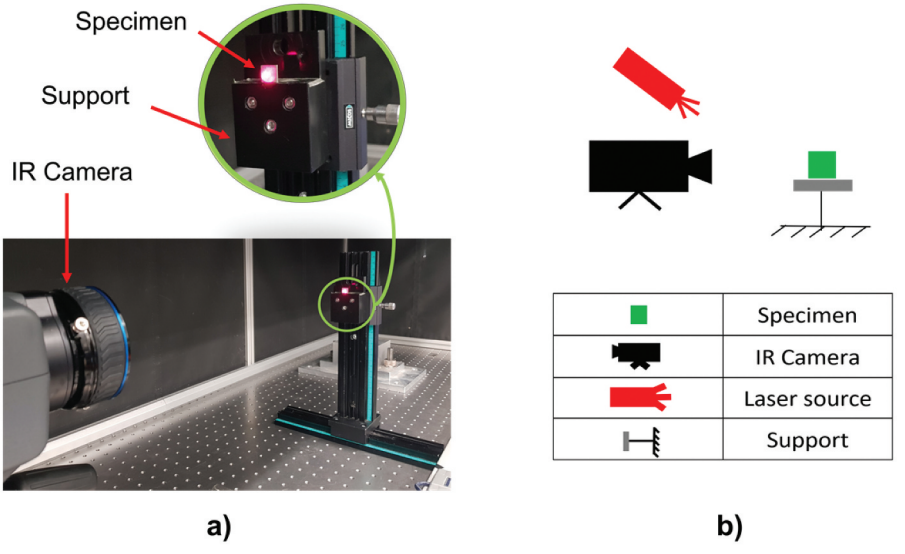

Figure 3. (a) at equipment; (b) schematic testing configuration.

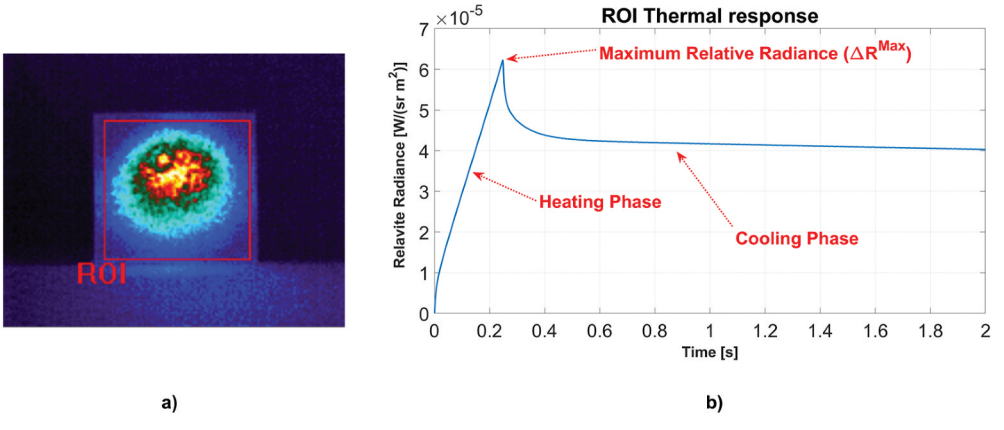

Figure 4. (a) ROI; (b) thermal response example: relative radiance.

The relative radiance profile (ΔR_r) (difference between measured radiance and room radiance) was computed for each specimen (see Figure 4(b)). Thermal responses generated from each specimen were compared and results were correlated with CS deposition temperatures and HEA chemical compositions. The Maximum Relative Radiance (ΔR_{Max}) value was chosen as the optimal parameter for the process characterisation. ΔR_{Max} corresponds to the maximum relative radiance (ΔR_r) value generated at the end of the heating phase (see Figure 4(b)).

3. Results and discussion

Experimental results are illustrated in this section where effects of HEA chemical composition variations and process temperature on the ΔR_{Max} peak and the corresponding roughness were investigated.

An example of the thermograms during the heating phase, for each sample, is detailed in Figure 5. Relative radiance (ΔR_r) heating and cooling profiles for each tested samples are compared in Figure 6, while the corresponding ΔR_{Max} values are collected in Table 3, which values are also represented in Figure 7 vs process temperature.

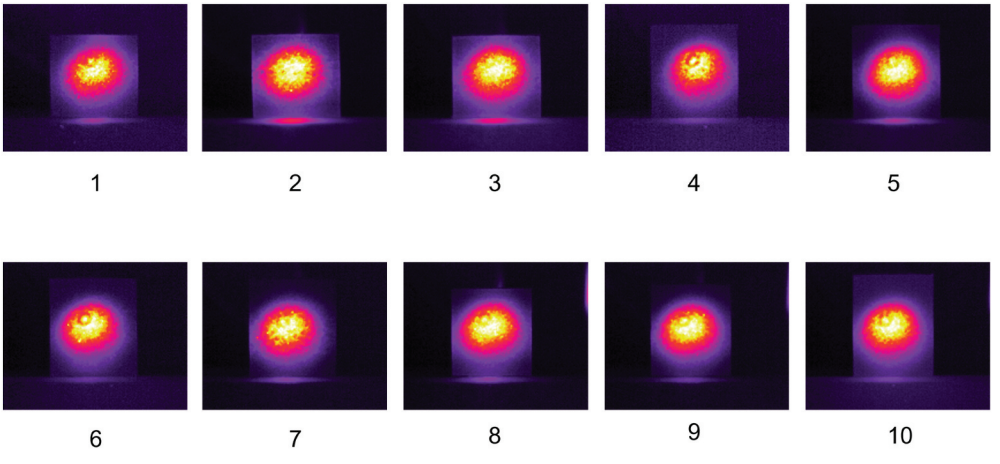

Figure 5. Thermograms for each sample during the heating phase (0.125 ms from thermal impulse).

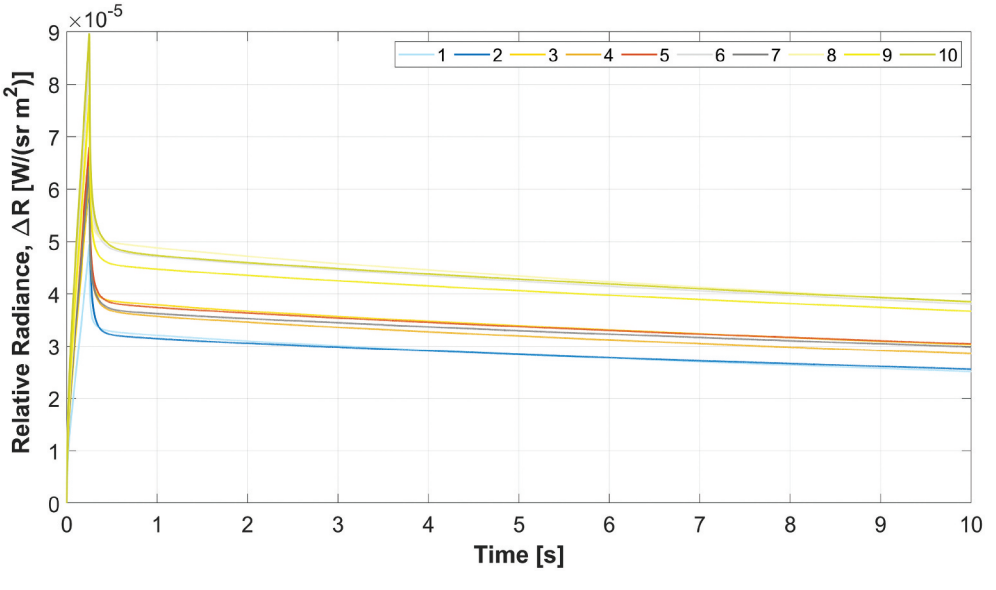

Figure 6. Relative radiance profiles (ΔR_r): Al0.1CoCrCuFeNi (blue), Al0.2CoCrCuFeNi (orange), Al0.5CoCrCuFeNi (grey), MnCoCrCuFeNi (yellow).

Table 3. Maximum relative radiance (ΔR_{Max}) of each sample.

			Maximum Relative Radiance (ΔR_{Max})	
Sample	Chemical composition	Cold Spray Temperature [°C]	Peak value [x 10^{-5} W/(sr m^2)]	Standard Deviation [x 10^{-5} W/(sr m^2)]
1	$Al_{0.1}CoCrCuFeNi$	650	4.95	0.02
2		750	6.11	0.03
3	$Al_{0.2}CoCrCuFeNi$	650	6.22	0.03
4		750	6.56	0.04
5		850	6.83	0.03
6	$Al_{0.5}CoCrCuFeNi$	650	8.49	0.03
7		750	6.45	0.03
8	MnCoCrCuFeNi	650	7.675	0.008
9		750	7.81	0.04
10		850	9.02	0.05

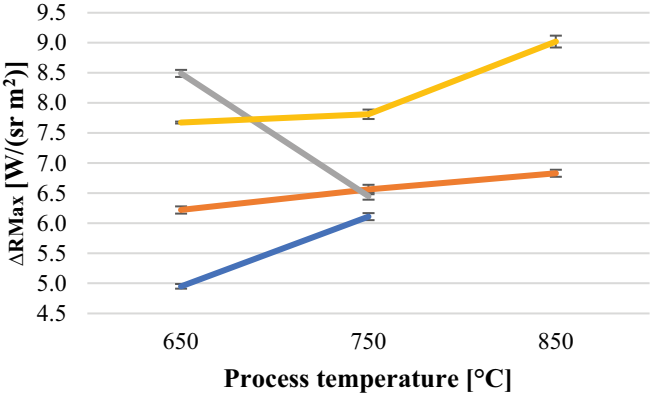

Figure 7. Maximum relative radiance (ΔR_{max}) vs cold spray deposition temperature variations: Al0.1CoCrCuFeNi (blue), Al0.2CoCrCuFeNi (orange), Al0.5CoCrCuFeNi (grey), MnCoCrCuFeNi (yellow).

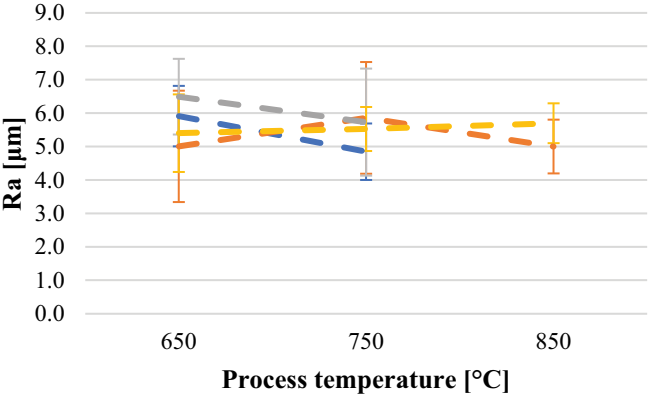

Figure 8. Surface roughness vs cold spray deposition temperature variations: Al0.1CoCrCuFeNi (blue), Al0.2CoCrCuFeNi (orange), Al0.5CoCrCuFeNi (grey), MnCoCrCuFeNi (yellow).

The roughness impact on the ΔR_{Max} variation was also investigated in Figures 8 and 9. More in detail, the roughness generated from the combination of possible CS deposition temperatures and HEA chemical compositions was compared with the corresponding

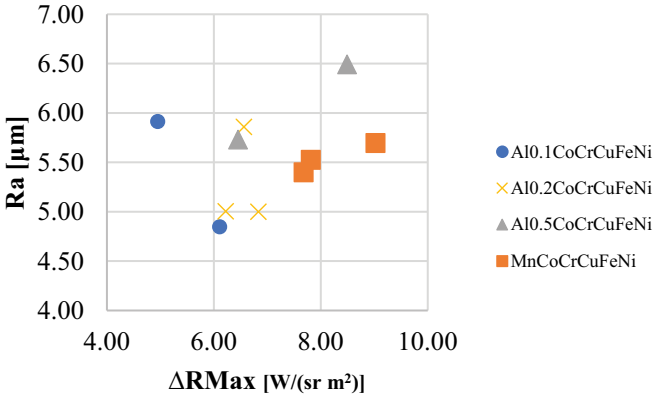

Figure 9. Maximum relative radiance vs roughness Ra for investigated specimens.

thermal response ΔR_{Max}. From the analysis of Figures 6 and 7 the effects of both CS deposition temperatures and HEA chemical compositions on the deposited coating radiance can be discussed. In Figure 6 the heating and cooling profiles are reported for the same energy laser excitation. It can be observed that the maximum relative radiance of Mn specimens is generally higher than Al specimens and this result can be related to the thermal properties of Mn alloys vs Al alloys. In [47–50] it is reported the dramatic difference in thermal conductivity of Al with respect to Mn, which is more than 100 times lower, while emissivity of Al is nearly half of Mn one; then the conduction phenomena in Al coatings are more effective in decreasing the maximum temperature after thermal impulse than what happens in Mn coating. The relation with process temperature can be justified if considering that process temperature affects the microstructure of the coating but is not related to surface roughness, as stated in [34]. Effects of CS deposition temperature on maximum relative radiance are highlighted in Figure 7. Scatter bars for a confidence interval of 95% are shown in the same plot.

A global ΔR_{Max} increment can be observed for the $Al_{0.1}$CoCrCuFeNi (Samples 1 and 2), $Al_{0.2}$CoCrCuFeNi (Samples 3, 4 and 5) and MnCoCrCuFeNi (Samples 8, 9 and 10) chemical composition, while the $Al_{0.5}$CoCrCuFeNi (Samples 6 and 7) chemical composition shows an opposite trend. As well known in literature, process temperature (CS deposition temperatures, 650°C – 750°C – 850°C) seems to impact on coating microstructure, even if its chemical composition remains the same. This result is confirmed by present results, that are different thermal responses generated from tested samples.

It can be concluded that with increasing process temperature, the ΔR_{Max} increases. Only for $Al_{0.5}$CoCrCuFeNi specimens, the ΔR_{Max} value decreases with process temperature, but this trend can be justified by the high value of surface roughness *Ra* of the 650°C processed specimens, the highest among all specimens (see Table 2).

As regard the influence of chemical composition, effects of different HEA chemical composition on the deposited coating are emphasised by the ΔR_{Max} peaks variations. In particular, Al percentage increment ($Al_{0.1}$, $Al_{0.2}$ and $Al_{0.5}$) generates different relative radiance responses. In case of 650°C Cold Spray deposition temperature, ΔR_{Max} peaks rise with the corresponding Al_x percentage

increment (Samples 1, 3 and 6). Similarly, for a 750°C CS deposition temperature, the effect of an Al_x percentage increment (Samples 3, 4 and 7) can be recognised with the ΔR_{Max} peaks variation. In this case, peaks generated by $Al_{0.2}$ and $Al_{0.5}$ HEA chemical composition (Samples 4 and 7) are comparable. Probably, the CS process generates coatings with similar properties, and, in consequence, a lower thermal response variation was measured.

The accuracy of the proposed process characterisation was guaranteed by the uncertainty bars detailed in Table 3. As a matter of fact, the bars regarding the Active Thermography results (see Figure 7) allowed the reproducibility of the ΔR_{Max} on the basis of the tested sample. Consequently, the influence of the process temperature and the chemical composition can be detected by using this alternative Non-Destructive setup.

In Figure 8 the roughness *Ra* vs CS temperatures for investigated specimens is plotted as an example. No apparent relation is pointed out. Figure 9 plots, for each sample, the measured roughness (*Ra* parameter) with the corresponding thermal response ΔR_{Max}. In [4] it resulted that specimens in $Al_{0.1}$CoCrCuFeNi show a decrease in all roughness parameters with increasing deposition temperature. For other specimens, a monotonic relationship between the roughness parameters and the temperature of the deposition process cannot be stated. Based on the experimental data obtained, it cannot be concluded that the chemical composition coupled with process temperature of the HEA influences the roughness of the coating. As mentioned in literature discussion, surface roughness can affect emissivity of a surface but in the present research the entity of the variation of roughness, according to literature evidence, does not result to affect emissivity and then surface radiance.

A dedicated Analysis of Variance (ANOVA) was performed on Al_xCoCrCuFeNi samples to investigate the significance level of both the CS deposition temperature and the HEA chemical composition on the ΔR_{Max} variation. On the basis of the available samples, $Al_{0.1}$CoCrCuFeNi and $Al_{0.5}$CoCrCuFeNi were chosen as levels for the Al chemical composition factor, while 650°C and 750°C CS were referred to the CS deposition temperature levels. This way, an Analysis of Variance (ANOVA) with two factors (the CS deposition temperature and the Al chemical composition) and with two levels for each factor ($Al_{0.1}$CoCrCuFeNi – $Al_{0.5}$CoCrCuFeNi for the HEA chemical composition factor, 650°C – 750°C for the CS deposition temperature factor) was performed on samples 1, 2, 6 and 7.

The ANOVA Statistical Analysis was performed by Minitab software. The Analysis of Variance and Pareto Chart are illustrated on Figure 10 and the analysis was performed with a confidence level of 95%. Assumptions, for ANOVA results validation, were completely verified in both the Normal Probability Plot and the Residual Analysis (Figure 11). Graphical results regarding the Analysis of Variance are illustrated in Figure 12. In particular, the main effect plot, the interaction plot, the contour plot and the surface plot for the ΔR_{Max} response are shown on the basis of the investigated factors. Globally, obtained results highlight a significant impact for both factors and their interaction on the ΔR_{Max} variation, statistically emphasised with *p*-value parameters less than 0.05.

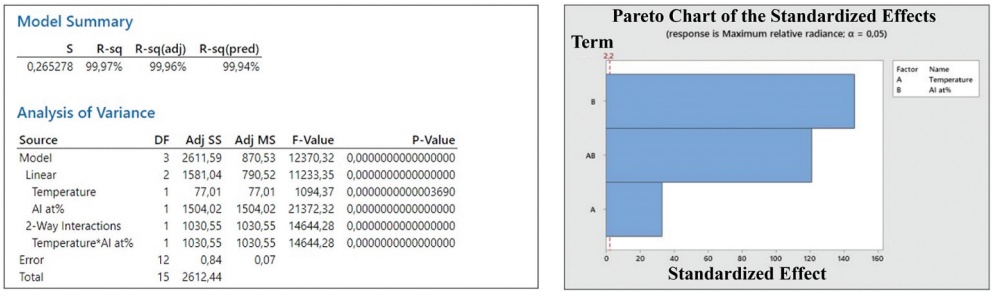

Model Summary

S	R-sq	R-sq(adj)	R-sq(pred)
0,265278	99,97%	99,96%	99,94%

Analysis of Variance

Source	DF	Adj SS	Adj MS	F-Value	P-Value
Model	3	2611,59	870,53	12370,32	0,0000000000000000
Linear	2	1581,04	790,52	11233,35	0,0000000000000000
Temperature	1	77,01	77,01	1094,37	0,0000000000003690
Al at%	1	1504,02	1504,02	21372,32	0,0000000000000000
2-Way Interactions	1	1030,55	1030,55	14644,28	0,0000000000000000
Temperature*Al at%	1	1030,55	1030,55	14644,28	0,0000000000000000
Error	12	0,84	0,07		
Total	15	2612,44			

Figure 10. Analysis of variance and Pareto Chart.

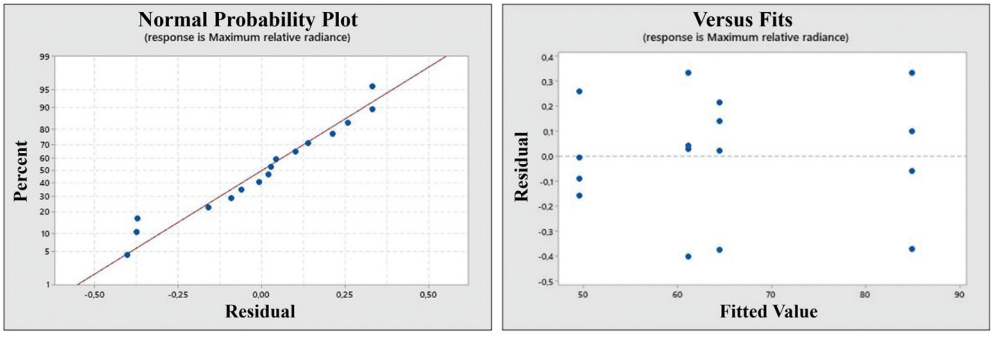

Figure 11. Normal probability plot and residual analysis.

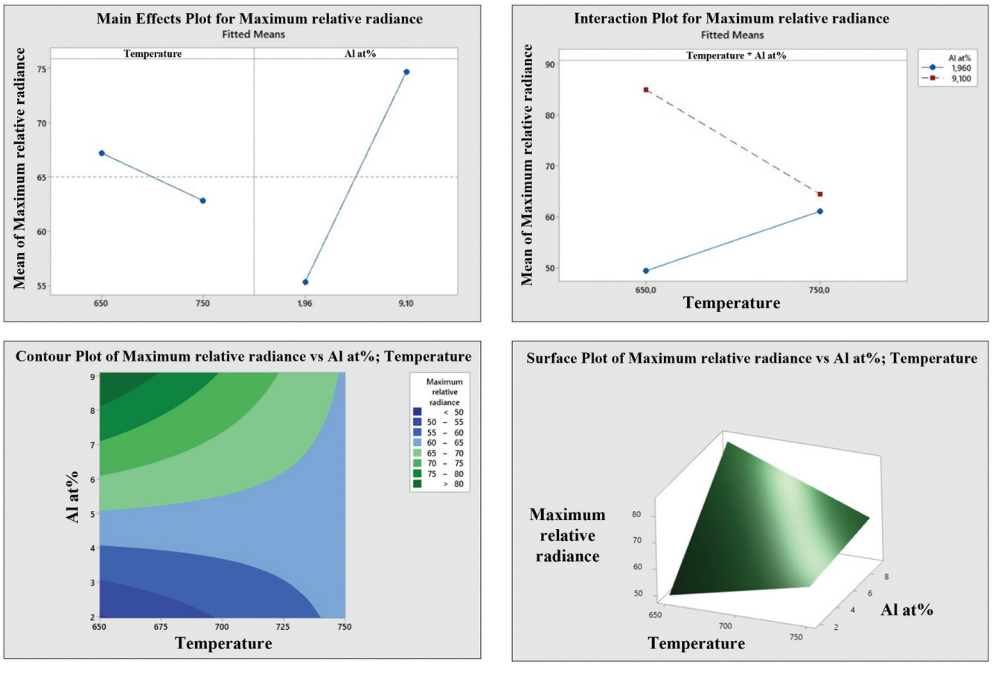

Figure 12. Analysis of variance results.

4. Conclusions

Paper aimed at investigating coating thermal response, in Active Thermography testing, with cold spray process parameters, for Al and Mn HEA cold sprayed coatings on Mg substrate.

To this aim, 4 materials (3 Al based and 1 Mn based HEA) and 3 cold spray temperatures were analysed. Surface roughness parameters (*Ra, Rq* and *Rt*) were measured.

Laser Pulsed Active Thermography was applied to obtain heating and cooling surface temperature profiles. An ANOVA statistical study was then performed on obtained results to point out correlations.

The following conclusions can be driven.

With increasing process temperature, the surface temperature increases, following the same laser excitation. In only one case, $Al_{0.5}CoCrCuFeNi$, the surface temperature decreases with process temperature due to the high value of surface roughness *Ra* of the 650°C processed specimen. No apparent relation is pointed out between surface roughness and cold spray process temperature.

The maximum relative radiance of Mn specimens is generally higher than Al specimens and this effect can be related to the thermal properties of Mn alloys vs aluminium alloys.

The investigation on the influence of chemical composition on maximum surface temperature showed that increasing the % of Al the surface temperature increased and Mn coating showed higher surface temperatures.

The ANOVA analysis run on Al specimens confirmed the obtained results with statistical evidence: a general decreasing effect on the ΔR_{Max} was observed by increasing the CS deposition temperature, while an opposite effect was shown for the Al chemical composition variation.

The proposed Active Thermography method was tested and statistically verified in case of samples covered with HEA coatings, and its validity for other types of coatings or different samples could be extended. The possible effects of the thickness of the coating or the shape of the specimen impact on the heat propagation (thermal responses) during the Active Thermography tests, requiring special attention when defining the heating source parameters. Future studies will be carried out with the aim of extending the proposed Non-Destructive Active Thermography method to different applications.

Acknowledgments

The authors would like to thank Francesco Artusio for his help as part of his Master thesis project.

The research mentioned here is funded by European Commission, REA through its Marie Swklodowska Curie European Individual Fellowship to one of the authors (SÖ), [Project No: 101018482] (Nov. 2021-Oct. 2023), which is gratefully acknowledged.

This publication is part of the project PNRR-NGEU which has received funding from the MUR-DM 352/2022

Disclosure statement

No potential conflict of interest was reported by the author(s).

Funding

The research mentioned here is funded by European Commission, REA through its Marie Swklodowska Curie European Individual Fellowship to one of the authors (SÖ), [Project No: 101018482] (Nov. 2021-Oct. 2023), which is gratefully acknowledged. This publication is part of the project PNRR-NGEU which has received funding from the MUR - DM 352/2022.

References

[1] Fotovvati B, Namdari N, Dehghanghadikolaei A, et al. On coating techniques for surface protection: a review. J Manuf Mater Process. 2019;3(1):28–. doi: 10.3390/jmmp3010028
[2] Yin S, Li W, Song B, et al. Deposition of FeCoNiCrMn high entropy alloy (HEA) coating via cold spraying. J Mater Sci Technol. 2019;35(6):1003–1007. doi: 10.1016/j.jmst.2018.12.015
[3] Tsai M-H, and Yeh J-W. High-Entropy Alloys: a critical review. Mater Res Lett. 2014;2 (3):107–123. doi: 10.1080/21663831.2014.912690
[4] Sesana R, Sheibanian N, Ozbilen S, et al. Cold spray hea coating surface microstructural characterization and mechanical testing. Results Mater. 2024;21:100540. doi: 10.2139/ssrn.4525757
[5] Wu Y, Zhang F, Yuan X, et al. Short-range ordering and its effects on mechanical properties of high-entropy alloys. J Mater Sci Technol. 2021;62:214–220. doi: 10.1016/j.jmst.2020.06.018
[6] Park JM, Choe J, Kim JG, et al. Superior tensile properties of 1%C-CoCrFeMnNi high-entropy alloy additively manufactured by selective laser melting. Mater Res Lett. 2020;8(1):1–7. doi: 10.1080/21663831.2019.1638844
[7] Li Z. Interstitial equiatomic CoCrFeMnNi high-entropy alloys: carbon content, microstructure, and compositional homogeneity effects on deformation behavior. Acta Materialia. 2019;164:400–412. doi: 10.1016/j.actamat.2018.10.050
[8] Luo H, Li Z, Mingers AM, et al. Corrosion behavior of an equiatomic CoCrFeMnNi High-entropy alloy compared with 304 stainless steel in sulfuric acid solution. Corros Sci. 2018;134:131–139. doi: 10.1016/j.corsci.2018.02.031
[9] Li R, Niu P, Yuan T, et al. Selective laser melting of an equiatomic CoCrFeMnNi High-entropy alloy: processability, non-equilibrium microstructure and mechanical property. J Alloys Compd. 2018;746:125–134. doi: 10.1016/j.jallcom.2018.02.298
[10] Cui Z, Qin Z, Dong P, et al. Microstructure and corrosion properties of FeCoNiCrMn high entropy alloy coatings prepared by high speed laser cladding and ultrasonic surface mechanical rolling treatment. Mater Lett. 2020;259:126769–. doi: 10.1016/j.matlet.2019.126769
[11] Löbel M, Lindner T, Lampke T, et al. High-temperature wear behaviour of AlCoCrFeNiTi0.5 coatings produced by HVOF. Surf Coat Technol. 2020;403:126379. doi: 10.1016/j.surfcoat.2020.126379
[12] Löbel M, Lindner T, Mehner T, et al. Microstructure and corrosion properties of AlCrFeCoNi high-entropy alloy coatings prepared by HVAF and HVOF. J Therm Spray Tech. 2022;31(1–2):247–255. doi: 10.1007/s11666-021-01255-2
[13] Medina LZ, Riekehr L, Jansson U, et al. Phase formation in magnetron sputtered CrMnFeCoNi high entropy alloy. Surf & Coat Technol. 2020;403:126323. doi: 10.1016/j.surfcoat.2020.126323
[14] Xiao J-K, Tan H, Wu Y-Q, et al. Microstructure and wear behavior of FeCoNiCrMn high entropy alloy coating deposited by plasma spraying. Surf Coat Technol. 2020;385:125430. doi: 10.1016/j.surfcoat.2020.125430
[15] Wang W, Zhang, Jiying B, et al. Study of high temperature friction and wear performance of (CoCrfemnni) 85Ti15 high-entropy alloy coating prepared by plasma cladding. Surf Coat Technol. 2020;384:125337. doi: 10.1016/j.surfcoat.2020.125337

[16] Chen C, Xie Y, Liu L, et al. Cold spray additive manufacturing of invar 36 alloy: microstructure, thermal expansion and mechanical properties. J Mater Sci Technol. 2021;72:39–51. doi: 10.1016/j.jmst.2020.07.038
[17] Yin S, Hassani M, Xie Q, et al. Unravelling the deposition mechanism of brittle particles in metal matrix composites fabricated via cold spray additive manufacturing. Scr Materialia. 2021;194:113614–. doi: 10.1016/j.scriptamat.2020.10.055
[18] Poza P, Ángel Garrido-Maneiro M. Cold-sprayed coatings: microstructure, mechanical properties, and wear behaviour. Prog Mater Sci. 2022;123:100839–. doi: 10.1016/j.pmatsci.2021.100839
[19] Wu D-Y, Zhou X, Li L-P, et al. Microstructure, mechanical properties and tribological behaviors of gold coating determined by surface quality. Surf Coat Technol. 2023;462:129463. doi: 10.1016/j.surfcoat.2023.129463
[20] Susoff M, Siegmann K, Pfaffenroth C, et al. Evaluation of icephobic coatings—screening of different coatings and influence of roughness. Appl Surf Sci. 2013;282:870–879. doi: 10.1016/j.apsusc.2013.06.073
[21] Nazir MH, Khan ZA, Stokes K, et al. Optimisation of interface roughness and coating thickness to maximise coating–substrate adhesion – a failure prediction and reliability assessment modelling. J Adhes Sci Technol. 2015;29(14):1415–1445. doi: 10.1080/01694243.2015.1026870
[22] Hainsworth SV, Page TF. Evaluation of the mechanical properties of ceramics and thin hard ceramic coatings using nanoindentation. Nondestr Test Evaluation. 2001;17(4–5):275–298. doi: 10.1080/10589750108953115
[23] Giurlani W, Berretti E, Innocenti M, et al. Measuring the thickness of metal coatings: a review of the methods. Coat (Basel). 2020;10(12):1211–. doi: 10.3390/coatings10121211
[24] Whiteside P, Chininis J, Hunt H. Techniques and challenges for characterizing metal thin films with applications in photonics. Coat (Basel). 2016;6(3):35–. doi: 10.3390/coatings6030035
[25] Doshvarpassand S, Wu C, Wang X, et al. An overview of corrosion defect characterization using active infrared thermography. Infrared Phys & Technol. 2019;96:366–389. doi: 10.1016/j.infrared.2018.12.006
[26] Usamentiaga R, Venegas P, Guerediaga J, et al. Infrared thermography for temperature measurement and non-destructive testing. Sensors. 2014;14(7):12305–12348. doi: 10.3390/s140712305
[27] Ibarra-Castanedo C, Tarpani JR, Maldague XPV, et al. Nondestructive testing with thermography. Eur J Phys. 2013;34(6):S91–109. doi: 10.1088/0143-0807/34/6/S91
[28] Ibarra-Castanedo C, Piau J-M, Guilbert S, et al. Comparative study of active thermography techniques for the nondestructive evaluation of honeycomb structures. Res Nondestr Evaluation. 2009;20(1):1–31. doi: 10.1080/09349840802366617
[29] Vavilov VP. Pulsed thermal NDT of materials: back to the basics. Nondestr Test Evaluation. 2007;22(2–3):177–197. doi: 10.1080/10589750701448407
[30] Bagavathiappan S, Lahiri BB, Saravanan T, et al. Infrared thermography for condition monitoring – a review. Infrared Phys & Technol. 2013;60:35–55. doi: 10.1016/j.infrared.2013.03.006
[31] Ma R, Dong L, Wang H, et al. Research on the contact fatigue failure of thermal sprayed coating based on infrared thermography. Nondestr Test Evaluation. 2020;35(1):73–97. doi: 10.1080/10589759.2019.1643866
[32] Piau J-M, Bendada A, Maldague X, et al. Nondestructive testing of open microscopic cracks in plasma-sprayed-coatings using ultrasound excited vibrothermography. Nondestr Test Evaluation. 2008;23(2):109–120. doi: 10.1080/10589750701775817
[33] Rachidi R, Elkihel B, Delaunois F, et al. Effectiveness of phased array focused ultrasound and active infrared thermography methods as a nondestructive testing of Ni-wc coating adhesion. Nondestr Test Evaluation. 2019;34(2):205–220. doi: 10.1080/10589759.2019.1566905

[34] Yang R, He Y, Zhang H, et al. Through coating imaging and nondestructive visualization evaluation of early Marine corrosion using electromagnetic induction thermography. Ocean Eng. 2018;147:277–288. doi: 10.1016/j.oceaneng.2017.09.023
[35] Zhang D, Yu Y, Lai C, et al. Thickness measurement of multi-layer conductive coatings using multifrequency eddy current techniques. Nondestr Test Evaluation. 2016;31 (3):191–208. doi: 10.1080/10589759.2015.1081903
[36] Cura F, Sesana R, Corsaro L, et al. Active thermography technique for barrier coatings characterization. IOP Conf Ser: Mater Sci Eng. 2022;1214(1):012034. doi: 10.1088/1757-899X/1214/1/012034
[37] Ozbilen S, Sesana R Sheibanian N, Vasquez JFB, Morris M, Lupoi R. Phase transformations/ separation via spinodal decomposition enhancing the structure & properties of MA+CS Al 0.1-0.5(Mn) CoCrCuFeNi HEA coatings on Mg vacuum annealed at 600oC. 2023. doi:10.2139/ssrn.4536207.
[38] Schwartz IB, Hon D. Emissivity as a function of surface roughness: A computer Model. Naval Research Lab. Report. 1986.
[39] Sabuga W, Todtenhaupt R. Effect of roughness on the emissivity of the precious metals silver, gold, palladium, platinum, rhodium, and iridium. High Temp High Pressures(uk). 2001;33(3):261–269.
[40] Seifter A, Boboridis K, Obst AW, et al. Emissivity measurements on metallic surfaces with various degrees of roughness: a comparison of laser polarimetry and integrating sphere reflectometry. Int J Thermophys. 2004;25(2):547–560. doi: 10.1023/B:IJOT.0000028489.81327.b7
[41] Ibos L, Marchetti M, Boudenne A, et al. Infrared emissivity measurement device: principle and applications. Meas Sci Technol. 2006;17(11):2950–2956. doi: 10.1088/0957-0233/17/11/013
[42] Wen C-D, Mudawar I. Modeling the effects of surface roughness on the emissivity of aluminum alloys. Int J Heat Mass Transf. 2006;49(23–24):4279–4289. doi: 10.1016/j.ijheatmasstransfer.2006.04.037
[43] Wang P, Xie, Z., Meng, H, et al. Effects of the temperature and roughness on the metal emissivity. In: The 27th Chinese Control and Decision Conference (2015 CCDC). Qingdao (China): IEEE; 2015. p. 6197–6200.
[44] Brodu E, Balat-Pichelin M, Sans J-L, et al. Influence of roughness and composition on the total emissivity of tungsten, rhenium and tungsten–25% rhenium alloy at high temperature. J Alloys Compd. 2014;585:510–517. doi: 10.1016/j.jallcom.2013.09.184
[45] Wu X, Wei X, Xu H, et al. Emissivity measurement based on deep learning and surface roughness. AIP Adv. 2021;11(8):085305–085305. doi: 10.1063/5.0055415
[46] Standard ISO 18434. Condition monitoring and diagnostics of machine systems thermography, part 2: image interpretation and diagnostics. International Standard Organization; 2019.
[47] Ross RB. Metallic Materials Specification Handbook. E. & FM Spon. London; 1992.
[48] Properties and Selection: Nonferrous Alloys and Special-Purpose Materials. ASM International 1990. ASM Handbook Committee.
[49] Alok N. The metals databook.New York: McGraw-Hill; 1997.
[50] Lide DR, editor. CRC handbook of chemistry and physics, 80th ed. Boca Raton (FL): CRC Press; 1999.